Original Article

Investigation of multichannel phased array performance for fetal MR imaging on 1.5T clinical MR system

Ye Li[1], Yong Pang[1], Daniel Vigneron[1,2], Orit Glenn[1], Duan Xu[1], Xiaoliang Zhang[1,2]

[1]Department of Radiology and Biomedical Imaging, University of California San Francisco, USA; [2]UCSF/UC Berkeley Joint Graduate Group in Bioengineering, San Francisco, CA, USA

Corresponding to: Xiaoliang Zhang, PhD. Department of Radiology and Biomedical Imaging, University of California San Francisco, Byers Hall, Room 102D, 1700 4th ST, San Francisco, CA 94158-2330, USA. Tel: 1-415-514-4801; Fax: 1-415-514-4451. Email: xiaoliang.zhang@ucsf.edu.

Abstract: Fetal MRI on 1.5T clinical scanner has been increasingly becoming a powerful imaging tool for studying fetal brain abnormalities *in vivo*. Due to limited availability of dedicated fetal phased arrays, commercial torso or cardiac phased arrays are routinely used for fetal scans, which are unable to provide optimized SNR and parallel imaging performance with a small number coil elements, and insufficient coverage and filling factor. This poses a demand for the investigation and development of dedicated and efficient radiofrequency (RF) hardware to improve fetal imaging. In this work, an investigational approach to simulate the performance of multichannel flexible phased arrays is proposed to find a better solution to fetal MR imaging. A 32 channel fetal array is presented to increase coil sensitivity, coverage and parallel imaging performance. The electromagnetic field distribution of each element of the fetal array is numerically simulated by using finite-difference time-domain (FDTD) method. The array performance, including B_1 coverage, parallel reconstructed images and artifact power, is then theoretically calculated and compared with the torso array. Study results show that the proposed array is capable of increasing B_1 field strength as well as sensitivity homogeneity in the entire area of uterus. This would ensure high quality imaging regardless of the location of the fetus in the uterus. In addition, the paralleling imaging performance of the proposed fetal array is validated by using artifact power comparison with torso array. These results demonstrate the feasibility of the 32 channel flexible array for fetal MR imaging at 1.5T.

Key Words: Fetal array; multichannel phased array; finite-difference time-domain; parallel imaging; MRI

Submitted Nov 08, 2011. Accepted for publication Nov 15, 2011.
DOI: 10.3978/j.issn.2223-4292.2011.11.04
Scan to your mobile device or view this article at: http://www.amepc.org/qims/article/view/60/46

Introduction

Fetal magnetic resonance imaging (MRI) on 1.5T clinical scanners has increasingly been performed to detect the brain abnormalities and potential neurodevelopmental disabilities since its first introduction in early 1980s (1-9). Due to fetal motion, multiecho ultrafast MRI techniques such as single-shot fast spin-echo (ssFSE) and half-Fourier acquired ssFSE are primarily used but at the price of signal-to-noise ratio (SNR) degradation. Parallel acquisition (10-12) and excitation, as a fast imaging technique, are feasible for fetal MRI with less focal SAR hot spots, higher SNR and reductions in scan time (13,14). However, since there are no dedicated fetal phased arrays available, commercial torso or cardiac phased arrays are routinely used instead, which are not optimized in SNR, safety and parallel imaging performance for fetal MRI, due to the limited coil elements, filling factor and B_1 field coverage. This poses a demand for investigation and development of dedicated radiofrequency (RF) hardware for efficient MR signal excitation and reception in fetal imaging.

Previous work demonstrates that well designed flexible transceiver arrays using microstrip elements (15-21) are feasible for various subjects with different sizes (22,23), which suggests the possibility of utilizing flexible phased array in fetal MRI. Current research has shown the significant SNR improvement in the region near the coil array as well as the deep region of a maternal body model by increasing the number of coil elements (24,25). By optimizing coil configuration and increasing coil elements, the filling factor and imaging coverage can be improved to achieve high SNR,

therefore, higher spatial resolution, sensitivity, and image homogeneity, and reduce scanning time in clinical fetal MRI.

Numerical calculation of RF electromagnetic fields in human models with realistic geometry and tissue properties using finite-difference time-domain (FDTD) algorithm is an efficient means in evaluating and optimizing coil configuration for better transmit/receive performance in MR imaging (26,27). The numerical calculation results lead to prospective insight into the coil performance for fetal MRI such as SNR, specific absorption rate (SAR) and parallel imaging feasibility, which provides important guideline for fetal array design and fabricating prototype coil arrays (28-32).

In this work, we propose a flexible 32-channel fetal phased array design to increase SNR, imaging coverage, parallel imaging performance and imaging safety in the whole uterus region. The performance of the proposed flexible array is investigated numerically and compared with the commercial 8-channel torso array at 1.5T. The B_1 field distribution of the proposed fetal array is analyzed by using FDTD method. In addition, GRAPPA reconstructed images with different acceleration factors are generated based on simulation results. Artifact power is measured to quantitatively evaluate parallel imaging performance.

Materials and methods

In order to improve imaging coverage and filling factor, the element number of dedicated fetal array increased to 32 while the size of each element was reduced correspondingly to cover the abdomen of mother. As shown in *Figure 1*, the fetal array consisted of 4×2 square surface coils with 110 mm width and 160 mm length on the bottom and 8×3 coils with 60 mm width and 70 mm length at the top except the four trapezoidal coil indicated by yellow arrows. By increasing the number of coil elements and the relative small size of each element, the array is more flexible, suitable for patients with different abdomen sizes and shapes. Compared with the 8-channel commercial torso array, which consisted of 4 square surface coils with 160 mm width and 160 mm length on the bottom and the other four with 110 mm width and 110 mm length at the top as shown in *Figure 1*, the coverage and filling factor were improved along with the increased flexibility.

The simulations of the two arrays were carried out using commercial FDTD software XFDTD 6.5 (REMCOM Inc., State College, PA) to compare array performance. The conductors (red region) were copper tapes (σ=5.8×10^7 S/m, μ_r=1 and 3 mm in width). The phantom (green region, σ=0.7 S/m and μ_r=72) was ellipse cylinder with 800 mm length, 205 mm long axel and 120 mm short axel, combined with a sphere with 140 mm radius. In order to achieve better coverage and filling factor, the coil elements at the top of the torso array were rotated 15° along the anterior-posterior direction. All the elements of the proposed fetal array were placed close to the phantom. A three-dimension FDTD simulation was performed at 64 MHz, corresponding to the proton Larmor frequency at 1.5T. Each element of the two arrays was excited by sinusoidal current source with RMS value of 1A and the same phase. Outer boundaries were absorbing perfectly matched layer (PML) with 7 layers. The meshing cells of the two models were 3 mm × 3 mm × 5 mm.

To evaluate the parallel imaging performance of the fetal array, GRAPPA (12,33-35) algorithm was utilized for image reconstruction. The electromagnetic field distribution of each element coil was simulated separately. The images of each element were calculated pixel by pixel based on simulation results. Ignoring relaxation and susceptibility effects, the gradient echo image intensity SI is given by (36,37).

$$SI = C\sin(\left|B_1^+\right|\gamma\tau)(\left|B_1^{-*}\right|) \quad [1]$$

where C is constant proportional to resonance frequency and initial magnetization, γ is the magnetogyric ratio, τ is the RF pulse duration, B_1^+ and B_1^- denote the positive and negative circularly polarized component respectively and the asterisk denotes a complex conjugate operation (38,39). As the phantom is assumed to be uniformly excited, *SI* is proportional to $|B_1^{-*}|$ according to equation [1]. A second order polynomial fit is performed to smooth the images.

The GRAPPA reconstruction was carried out by using PULSAR toolbox (40). 32 Auto-Calibration Signal (ACS) lines in the center of the k-space were used to estimate the missing lines. The block size was 2. All the coils were used for GRAPPA reconstruction. The coil distribution was set to linear. 90% of k-space along frequency-encoding direction was employed for fitting. The GRAPPA reconstruction with subsampling factors of 2, 4, 6 and 8, corresponding to acceleration factors of 1.7, 2.6, 3.2 and 3.5 respectively, was performed to A/P direction in axial plane. Sum-of-square (SoS) images were calculated as reference (41).

Results

The B_1 field distributions in the transversal and sagittal planes of the two arrays, which was scaled to 2×10^{-7} W input power of each element, was shown in *Figure 2* and *3*. The mean B_1 in 3 cm × 3 cm region at different location in the whole uterus was shown in the black boxes. As shown in *Figure 2*, B_1 was increased 20% in the surface region at the center of transversal plane, whilst that on left and right sides increased 40% to 180% due to the better coverage of the

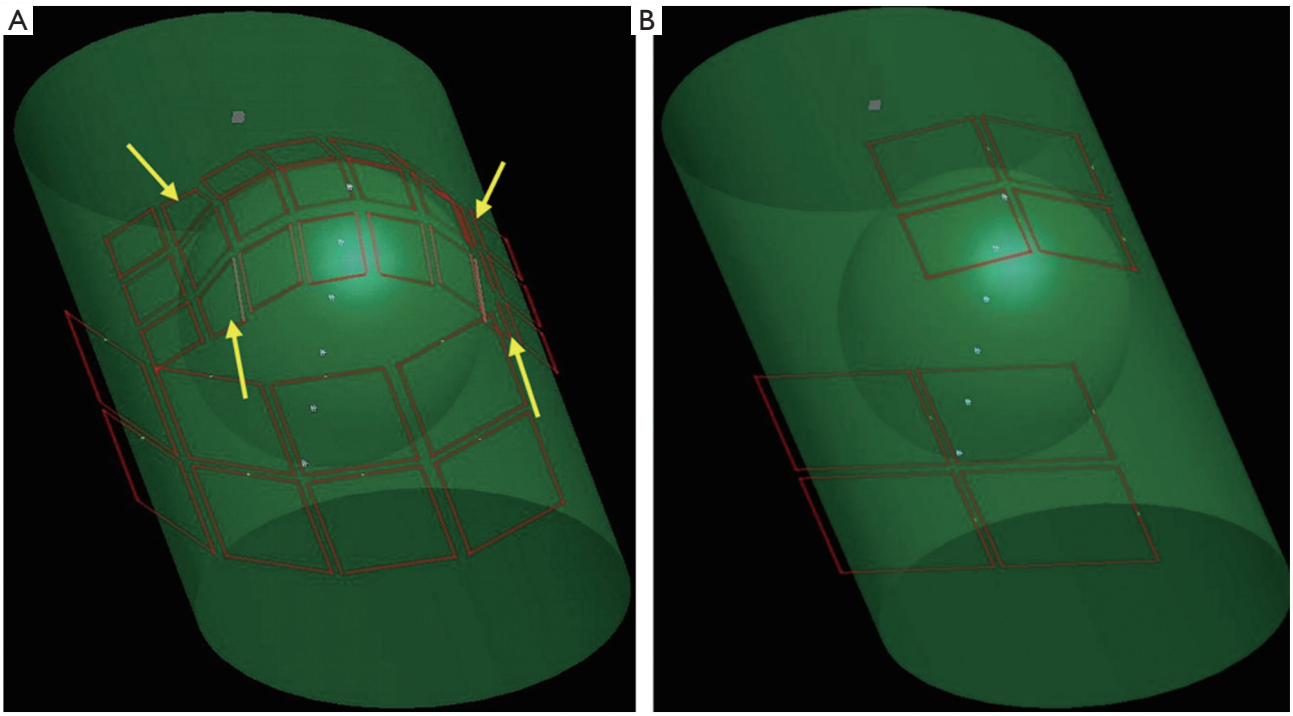

Figure 1 Configurations of coils and phantoms, 32 channel fetal array (A) and 8 channel torso array (B)

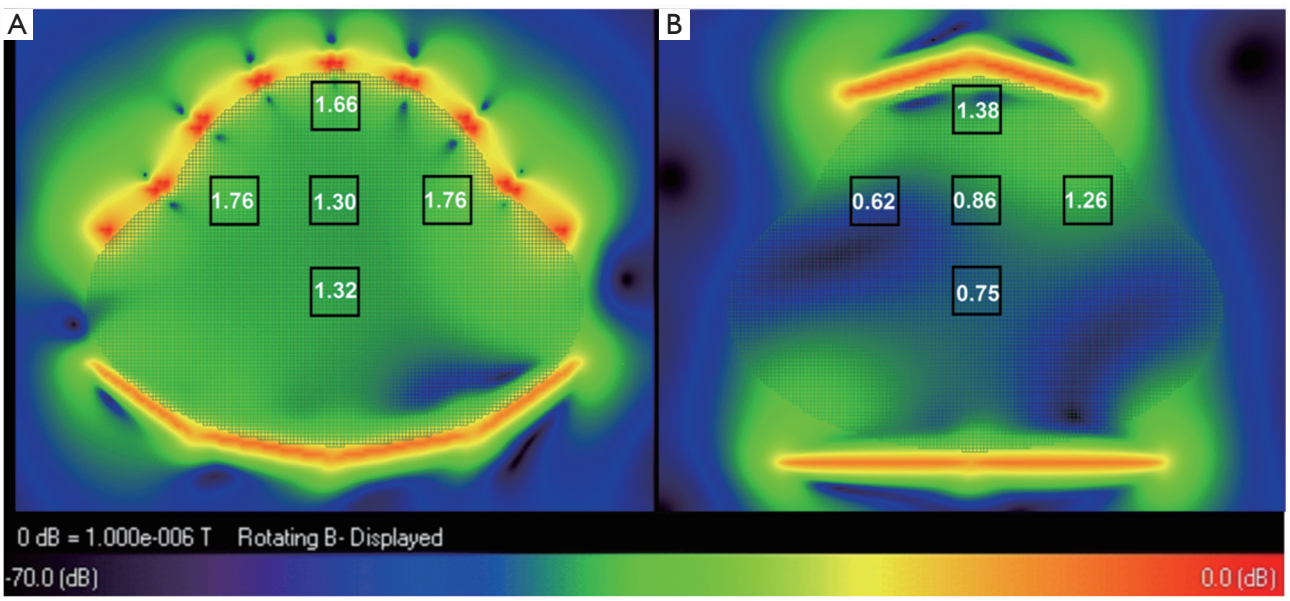

Figure 2 *B1* map of (A) 32 channel fetal array and (B) 8 channel torso array in the central transversal plane of the phantom calculated by XFDTD. The numbers in the boxes indicated the mean B1 (10^{-8}T) in the 3 cm × 3 cm region

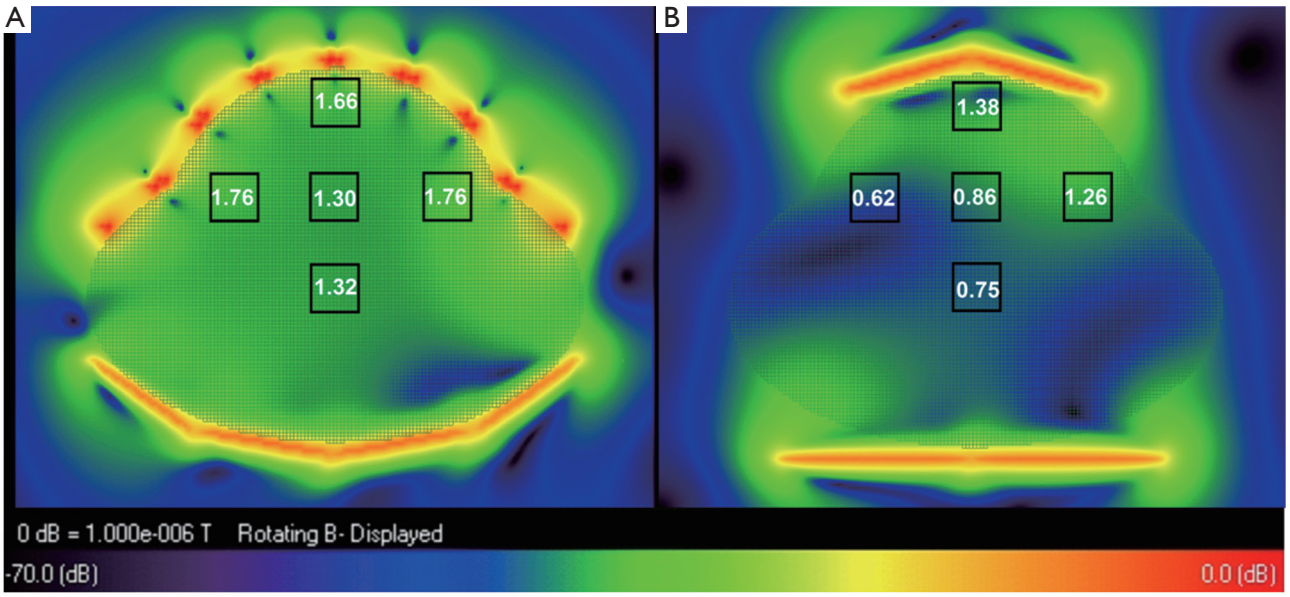

Figure 3 *B1* map of (A) 32 channel fetal array and (B) 8 channel torso array in the central sagittal plane of the phantom calculated by XFDTD. The numbers in the boxes indicated the mean B1 (10^{-8}T) in the 3 cm × 3 cm region

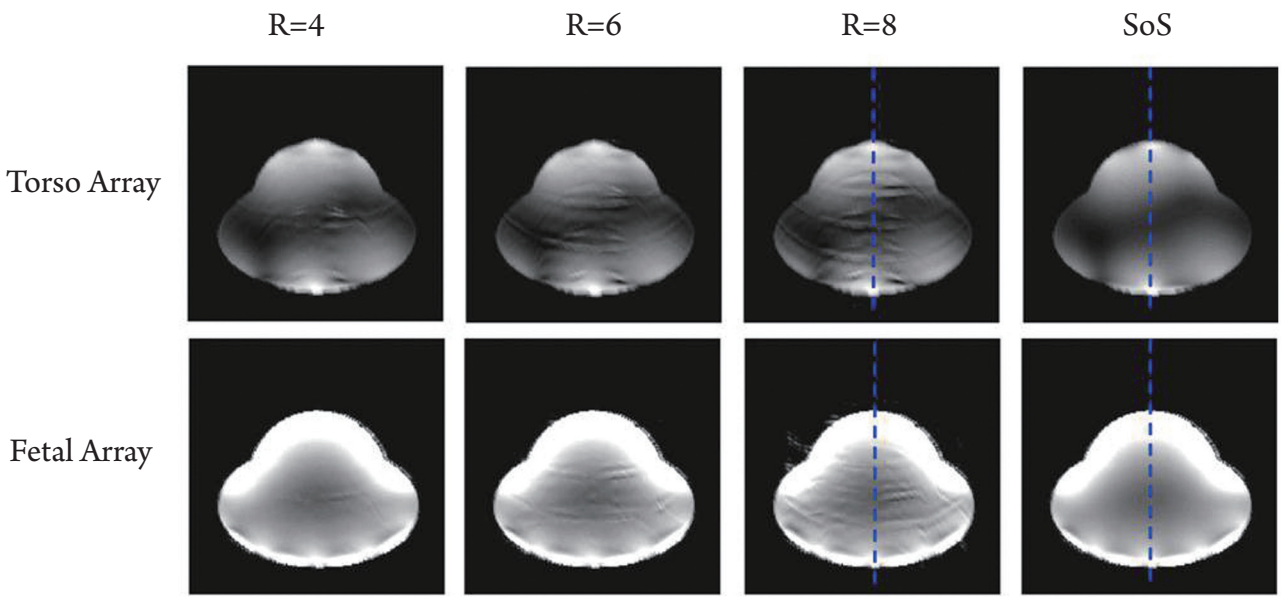

Figure 4 GRAPPA reconstructed images. 32 Auto-Calibration Signal (ACS) lines in the center of the k-space were used to estimate the missing lines. The GRAPPA reconstruction with acceleration factors of 1.7, 2.6, 3.2 and 3.5 was performed to A/P direction in axial plane

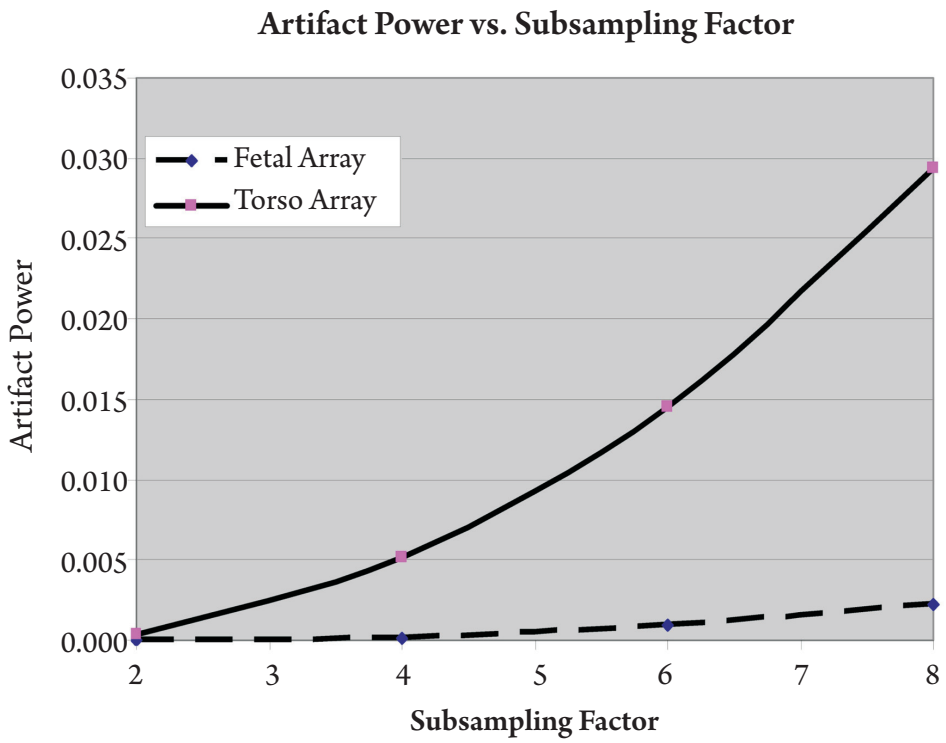

Figure 5 Artifact power comparison between fetal array and torso array with subsampling factors of 2, 4, 6, and 8

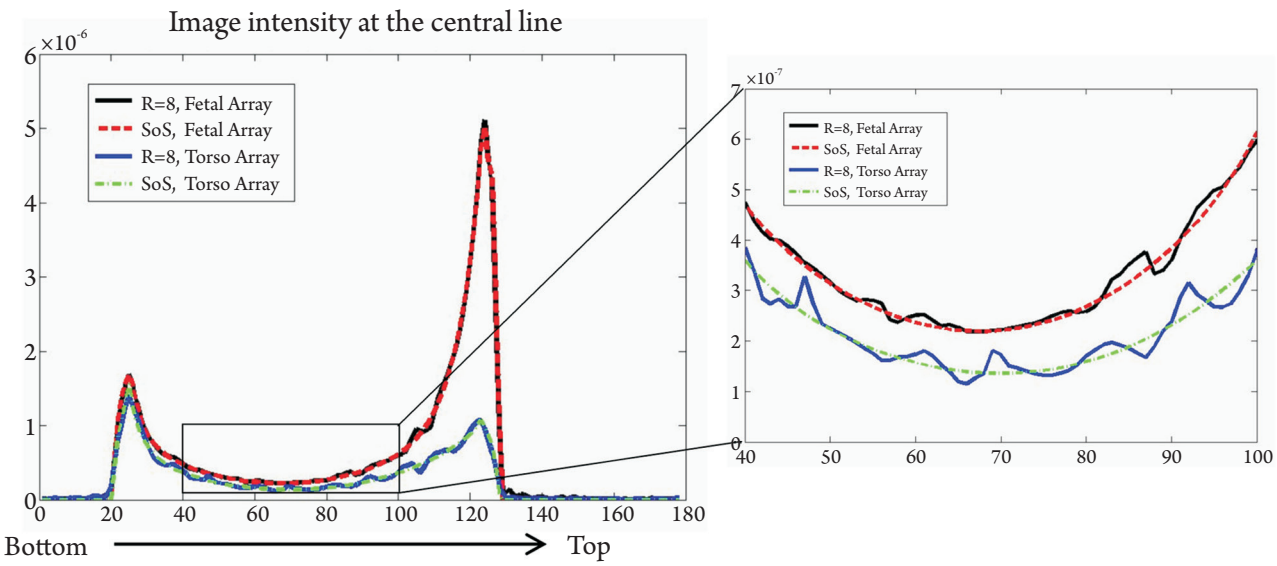

Figure 6 The image intensity of SoS and GRAPPA reconstructed images with subsampling factor 8 at the center lines (blue dash lines in Figure 4). The right figure is zoom-in image, showing image intensity in deeper region in uterus

32 channel fetal array. As shown in *Figure 3*, B_1 increased 50% in the center of surface region as well as that on the anterior and posterior sides was increased 28% due to better filling factor of the fetal array. B_1 in the center of uterus and in deeper region such as the center of the patient was increased 87% and 79% respectively because of increasing the number of element. Besides the improvement of B_1 field strength, the sensitivity homogeneity also increased substantially which is important for fetal MRI due to the possibility of fetus head location in the whole uterus.

The GRAPPA and sum-of-square reconstructed images were shown in *Figure 4*. The first row was the images of eight-channel torso array and the second row was of 32-channel fetal array. Artifact power was calculated to quantitatively evaluate the parallel imaging performance of two arrays. The artifact power (AP) was defined as (40).

$$AP = \sum_{x,y} \frac{\left\| I^{SoS}(x,y) \right| - c \left| I^{GRAPPA}(x,y) \right\|^2}{\left| I^{SoS}(x,y) \right|^2} \quad [2]$$

where I^{SoS} and I^{GRAAPA} were the image intensity of sum-of-square images and GRAPPA reconstructed images. As shown in *Figure 5*, the fetal array dramatically reduced the artifact power compared with the torso array. The artifact power of fetal array with subsampling factor 8 was diminished to 7.8% of that of torso array. Figure 6 showed the image intensity of SoS and GRAPPA reconstructed images with subsampling factor 8 at the center line, which demonstrated the image intensity of the fetal array increased 5-fold in surface region. The zoom-in image in *Figure 6* showed 50% improvement in the deeper region compared with that of torso array, although the sizes of each element of the fetal array were smaller than torso array (42).

Conclusions and Discussions

This study indicates the proposed 32-channel fetal array improves SNR, sensitivity homogeneity and imaging coverage by increasing the number of array element. The artifact of parallel reconstructed images is reduced dramatically by using the proposed flexible fetal array. These results demonstrate the feasibility of the 32 channel flexible array and the performance improvement over the torso or cardiac array, providing a more sensitive, faster and safer imaging method for fetal MR imaging at 1.5T.

Some B_1 drop-off near the surface of maternal body model as shown in *Figure 2* and *Figure 3* can be observed. This field distribution can be further improved by performing B_1 shimming with the fetal array or fine adjusting the phase and amplitude on the array elements, or even by simple post-processing during the image reconstruction. This certainly deserves a further study.

With the use of multichannel RF transmitter, the flexible fetal array can be also used as a transmit/receive array to perform regularly transmitting or parallel excitation for B_1 filed shimming and fast selective excitation. Since the region of interest is relatively smaller than the maternal abdomen, the excitation power can be reduced by using transmit array instead of regular body coil. Therefore, the average SAR and resulting temperature rise will decrease which improves patient safety.

Acknowledgements

This work was supported in part by NIH grants EB004453, EB008699, EB007588-03S1 and P41EB013598, and a QB3 Research Award, and UCSF Radiology seed grant (10-41).
Disclosure: The authors declare no conflict of interest.

References

1. Simon EM, Goldstein RB, Coakley FV, et al. Fast MR imaging of fetal CNS anomalies in utero. AJNR Am J Neuroradiol 2000;21:1688-98.
2. Coakley FV, Glenn OA, Qayyum A, et al. Fetal MRI: a developing technique for the developing patient. AJR Am J Roentgenol 2004;182:243-52.
3. Prayer D, Brugger PC, Prayer L. Fetal MRI: techniques and protocols. Pediatr Radiol 2004;34:685-93.
4. Glenn OA, Barkovich AJ. Magnetic resonance imaging of the fetal brain and spine: an increasingly important tool in prenatal diagnosis, part 1. AJNR Am J Neuroradiol 2006;27:1604-11.
5. Glenn OA, Barkovich J. Magnetic resonance imaging of the fetal brain and spine: an increasingly important tool in prenatal diagnosis: part 2. AJNR Am J Neuroradiol 2006;27:1807-14.
6. Prayer D, Kasprian G, Krampl E, et al. MRI of normal fetal brain development. Eur J Radiol 2006;57:199-216.
7. Garel C. Fetal MRI: what is the future? Ultrasound Obstet Gynecol 2008;31:123-8.
8. Glenn OA. Normal development of the fetal brain by MRI. Semin Perinatol 2009;33:208-19.
9. Limperopoulos C, Clouchoux C. Advancing fetal brain MRI: targets for the future. Semin Perinatol 2009;33:289-98.
10. Sodickson DK, Manning WJ. Simultaneous acquisition of spatial harmonics (SMASH): fast imaging with radiofrequency coil arrays. Magn Reson Med 1997;38:591-603.
11. Pruessmann KP, Weiger M, Scheidegger MB, et al. SENSE: sensitivity encoding for fast MRI. Magn Reson Med 1999;42:952-62.
12. Griswold MA, Jakob PM, Heidemann RM, et al. Generalized

autocalibrating partially parallel acquisitions (GRAPPA). Magn Reson Med 2002;47:1202-10.
13. Herlihy D, Larkman DJ, Allsop J, et al. A flexible highly configurable 16 channel array coil for fetal imaging. Proc Intl Soc Mag Reson Med 17 2009;2971.
14. Filippi CG, Johnson A, Nickerson JP, et al. Fetal Imaging with Multitransmit MR at 3.0T: Preliminary Findings. Aviable online: http://eta2.bio.cmu.edu/ISMRM/ISMRM%20 2010%20Stockholm/files/2023_2441.pdf
15. Zhang X, Ugurbil K, Chen W. Microstrip RF surface coil design for extremely high-field MRI and spectroscopy. Magn Reson Med 2001;46:443-50.
16. Lee RF, Westgate CR, Weiss RG, et al. Planar strip array (PSA) for MRI. Magn Reson Med 2001;45:673-83.
17. Zhang X, Ugurbil K, Sainati R, et al. An inverted-microstrip resonator for human head proton MR imaging at 7 tesla. IEEE Trans Biomed Eng 2005;52:495-504.
18. Zhang X, Ugurbil K, Chen W. A microstrip transmission line volume coil for human head MR imaging at 4T. J Magn Reson 2003;161:242-51.
19. Adriany G, Van de Moortele PF, Wiesinger F, et al. Transmit and receive transmission line arrays for 7 Tesla parallel imaging. Magn Reson Med 2005;53:434-45.
20. Zhang X, Ugurbil K, Sainati R, et al.An inverted-microstrip resonator for human head proton MR imaging at 7 tesla. IEEE Trans Biomed Eng 2005;52:495-504.
21. Zhang X, Zhu XH, Chen W. Higher-order harmonic transmission-line RF coil design for MR applications. Magn Reson Med 2005;53:1234-9.
22. Li Y, Xie Z, Pang Y, et al. ICE decoupling technique for RF coil array designs. Med Phys 2011;38:4086-93.
23. Wu B, Wang C, Krug R, et al. Multi-purpose Flexible Transceiver Array at 7T. Proc Intl Soc Mag Reson Med 17;2009:107
24. Lattanzi R, Grant AK, Polimeni JR, et al. Performance evaluation of a 32-element head array with respect to the ultimate intrinsic SNR. NMR Biomed 2010;23:142-51.
25. Wald LL. Parallel Imaging Update: How Many Elements Do We Need? Proc Intl Soc Mag Reson Med 14;2006:202.
26. Collins CM. Numerical field calculations considering the human subject for engineering and safety assurance in MRI. NMR Biomed 2009;22:919-26.
27. Yee KS. Numerical Solution of Initial Boundary Value Problems Involving Maxwells Equations in Isotropic Media. IEEE Trans. Antennas and Propagation 1966;14:302-7.
28. Hand JW, Li Y, Thomas EL, et al. Prediction of specific absorption rate in mother and fetus associated with MRI examinations during pregnancy. Magn Reson Med 2006;55:883-93.
29. Nagaoka T, Togashi T, Saito K, et al. An anatomically realistic whole-body pregnant-woman model and specific absorption rates for pregnant-woman exposure to electromagnetic plane waves from 10 MHz to 2 GHz. Phys Med Biol 2007;52:6731-45.
30. Dimbylow PJ, Nagaoka T, Xu XG. A comparison of foetal SAR in three sets of pregnant female models. Phys Med Biol 2009;54:2755-67.
31. Hand JW, Li Y, Hajnal JV. Numerical study of RF exposure and the resulting temperature rise in the foetus during a magnetic resonance procedure. Phys Med Biol 2010;55:913-30.
32. Li Y, Pang Y, Vigneron D, et al. Investigation of multichannel phased array configurations for fetal MR imaging at 1.5T. Proc Intl Soc Mag Reson Med 19;2011:2969.
33. Griswold MA, Blaimer M, Breuer F, et al. Parallel magnetic resonance imaging using the GRAPPA operator formalism. Magn Reson Med 2005;54:1553-6.
34. Park J, Zhang Q, Jellus V, et al. Artifact and noise suppression in GRAPPA imaging using improved k-space coil calibration and variable density sampling. Magn Reson Med 2005;53:186-93.
35. Wang Z, Wang J, Detre JA. Improved data reconstruction method for GRAPPA. Magn Reson Med 2005;54:738-42.
36. Hoult DI. The principle of reciprocity in signal strength calculations - A mathematical guide. Concepts in Magnetic Resonance 2000;12:173-87.
37. Hoult DI, Phil D. Sensitivity and power deposition in a high-field imaging experiment. J Magn Reson Imaging 2000;12:46-67.
38. Collins CM, Yang QX, Wang JH, et al. Different excitation and reception distributions with a single-loop transmit-receive surface coil near a head-sized spherical phantom at 300 MHz. Magn Reson Med 2002;47:1026-8.
39. Wang J, Yang QX, Zhang X, et al. Polarization of the RF field in a human head at high field: a study with a quadrature surface coil at 7.0 T. Magn Reson Med 2002;48:362-9.
40. Ji JX, Son JB, Rane SD. PULSAR: A Matlab toolbox for parallel magnetic resonance imaging using array coils and multiple channel receivers. Concepts in Magnetic Resonance Part B: Magnetic Resonance Engineering 2007;31B:24-36.
41. Roemer PB, Edelstein WA, Hayes CE, et al. The NMR phased array. Magn Reson Med 1990;16:192-225.
42. Ohliger MA, Sodickson DK. Sodickson. An introduction to coil array design for parallel MRI. NMR in Biomedicine 2006;19:300-15.

Cite this article as: Li Y, Pang Y, Vigneron D, Glenn O, Xu D, Zhang X. Investigation of multichannel phased array performance for fetal MR imaging on 1.5 T clinical MR system. Quant Imaging Med Surg 2011;1(1):24-30. DOI: 10.3978/j.issn.2223-4292.2011.11.04

